Griffiths, D. V. & Prevost, J. N. (1988). *Géotechnique* **38**, No. 3, 367–388

Two- and three-dimensional dynamic finite element analyses of the Long Valley Dam

D. V. GRIFFITHS* and J. H. PREVOST†

Earthquake response records from the well-instrumented Long Valley Dam in the Mammoth Lake area of California are compared with numerical prediction made using finite element models. The soil response to cyclic loading is accounted for by the use of a multi-surface plasticity model. The input and output to the finite element analyses take the form of accelerations at the base and at various crest locations. The computed and measured crest acceleration are compared in both the time and frequency domains. Natural frequencies have also been obtained for the finite element models and for the real structure. The time-domain results give good agreement and high correlation in the up/down-stream direction but poor agreement in the vertical direction. The failure of the finite element models to capture the high-frequencies present in the vertical and transverse directions is thought to be partly due to the crude finite element discretization used.

KEYWORDS: **constitutive relations; dams; dynamics; earthquakes; finite elements; plasticity.**

L'article compare les données de réponse aux tremblements de terre pour le barrage bien instrumenté de Long Valley dans la région du Mammouth Lake en Californie aux prédictions numériques faites à l'aide de modèles à éléments finis. La réponse du sol au chargement cyclique est expliquée grâce á d'un modèle de plasticité à surfaces multiples. Les données d'entrée et de sortie pour les analyses par éléments finis prennent la forme d'accélérations à la base et à différents emplacements de crête. Les accélérations de crête calculées et mesurees sont comparées pour le temps et pour les fréquences. On a obtenu aussi des fréquences naturelles pour les modèles en éléments finis et pour la structure réelle. Les résultats pour le temps et pour la fréquence s'accordent bien avec une bonne corrélation dans les directions en amont et en aval mais ne s'accordent que médiocrement pour la direction verticale. On pense que le fait que les modèles par éléments finis n'attrapent pas les hautes fréquences dans les directions verticale et transversale est dû en partie à la discrétization sommaire employée pour les éléments finis.

NOTATION

A, B	curve fitting parameters
c', ϕ'	effective shear strength parameters
dp/dq	gradient of p vs q
K_0, K_p	at rest, passive earth pressure coefficients
n	number of records
p	$(\sigma_1 + \sigma_2 + \sigma_3)/3$ mean stress
p_0, q_0	initial values
q	$(\sigma_1 - \sigma_3)$ shear stress
q_{max}	peak value
r_{xy}	correlation coefficient between x and y
s_{xy}	xy covariance
s_{xx}^2	x-sample variance
s_{yy}^2	y-sample variance
$\bar{x}$, $\bar{y}$	mean values
α, β	time-stepping parameters
Δt	time-step
$\bar{\varepsilon}$	$(\varepsilon_1 - \varepsilon_3)$ shear strain
ν_0, G_0, E_0	initial elastic parameters
τ	time-shift

INTRODUCTION

The response of earth dams to earthquake excitation is a complex process in which full account must be taken of the non-linear response of the soil skeleton to cyclic loading. The form of the assumed constitutive relations for the soils will depend to a large extent on the type of materials present in the dam and their relative permeabilities. In an earlier analysis on the Santa Felicia Dam (Lacy & Prevost, 1987), the embankments had a much higher permeability than the clay core, resulting in a steeply falling free-surface line. The saturated materials below the free-surface were treated by a fully coupled finite element analysis in which account was taken of

Discussion on this Paper closes on 1 January 1989. For further details, see p. ii.

* University of Manchester.
† Princeton University.

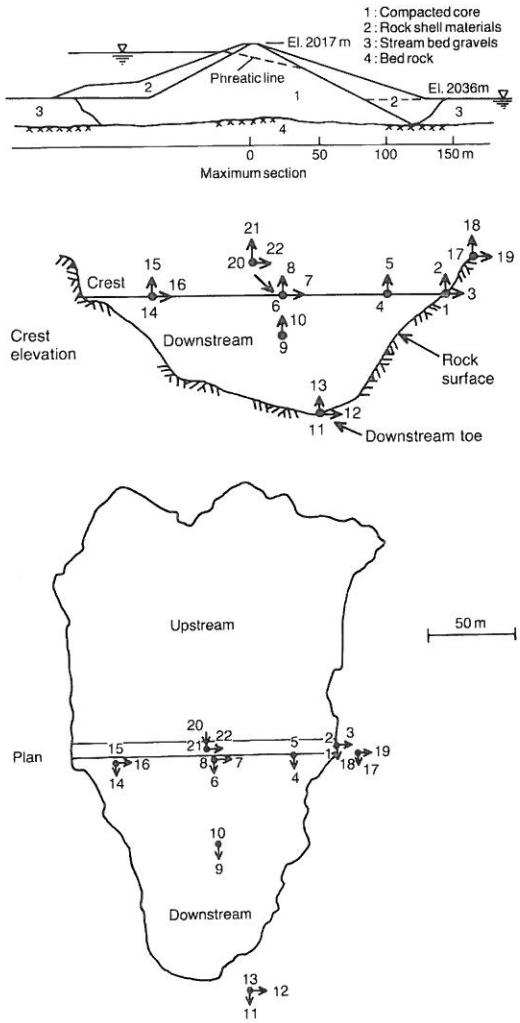

Fig. 1. Details of the Long Valley Dam and the location of strong motion instrumentation

the two-phase nature of the soil–water mixture. The two-phase approach was found to give a better response than the equivalent one-phase approach when compared with measured values from the field.

This Paper describes finite element analyses of the Long Valley Dam which consists of an extensive rolled earthfill core and compacted embankments of more permeable material. The extensive nature of the clay core means that the free-surface falls very gradually through the dam, hence the entire dam is essentially saturated. A two-phase analysis in this case is not required and so a one-phase approach is used in which the soil–water mixture is treated as a single composite material.

The Long Valley Dam (Hoye, Hegenbart & Matsuda, 1982) was constructed in the 1930's in a narrow canyon approximately 35 km north-west of Bishop, California. The dam has a maximum height above the valley floor of 54 m. In May 1980, the area was subjected to a series of earthquakes which triggered a number of accelerographs placed on or around the dam (Turpen, 1980). Figure 1 shows various sections of the dam and the location and orientation of the 22 accelerographs. The largest earthquake experienced by the dam occurred on 27 May 1980, resulting in peak abutment accelerations of 0·18 g, 0·09 g and 0·22 g and peak crest accelerations of 0·47 g, 0·19 g and 0·29 g in the x (up/downstream) y (vertical) and z (transverse) directions, respectively. Acceleration readings were made at 0·02 second intervals and a total duration of 12 s was used as input to the finite element analyses.

Previous analyses of the Long Valley Dam have been reported by Lai & Seed (1985). In these analyses, the non-linear characteristics of the dam behaviour were accounted for by using equivalent linear soil properties and an iterative procedure to obtain modulus and damping values compatible with the amount of straining computed in each zone of the soil mass. In the present analyses a more rigorous approach is used in which the nonlinear hysteretic behaviour of the dam materials is accounted for by using a multi-surface plasticity theory (Prevost, 1977). All reported calculations were performed by using the DYNAFLOW program (Prevost, 1981 and 1987).

FINITE ELEMENT DISCRETIZATION

Two dimensions

The widest section of the dam in the up/downstream direction was used as a basis for the two-dimensional finite element discretization shown in Fig. 2. The mesh has 215 nodes, 178 four-node elements and 352 degrees of freedom in the x and y directions. The mesh is divided into nine soil groups, each with different soil properties to reflect the spatial variation in stiffness and strength. Two groups represent the embankment shell material, six groups represent the clay core and one, the existing stream beds to the sides. The input accelerations were applied in the x and y directions to the 39 nodes at the base and extreme sides of the mesh. The input was taken from the corresponding measured acceleration from accelerographs 11 and 13 (Fig. 1 (b) and (c)). At each time step (Δt = 0·02 s) the x and y accelerations at all nodes in the mesh were computed from the non-linear finite element analysis. Of particular interest was the computed acceleration at the crest (node 111) which could be compared directly with measured values at accelerographs 20 and 21.

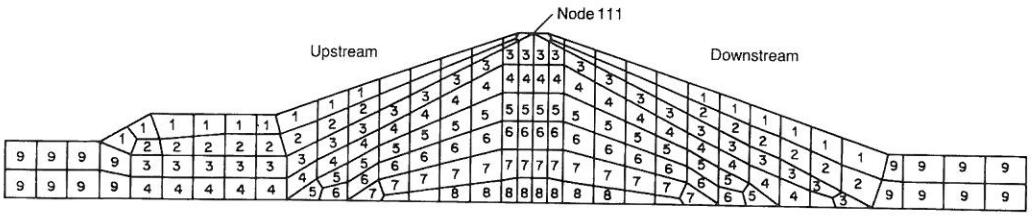

Fig. 2. Mesh used for two-dimensional analyses

Three dimensions

The Long Valley Dam is built in a relatively narrow canyon, and it was felt that the assumption of plane-strain conditions at the centreline might not be wholly justified. For this reason, a three-dimensional model of the dam was created as shown in Fig. 3. The mesh consists of 13 sections in the transverse direction, 878 nodes, 528 eight-node brick elements and 1620 degrees of freedom in the x, y and z directions and is symmetrical about the up/downstream centreline. In spite of the greater number of elements, the mesh contains only five soil groups; one in the shell, three in the core and one to the sides. This was felt to be a rather crude description of the spatial variation of soil properties. Input accelerations to the base and sides of the mesh were those recorded at stations 11, 13 and 12 respectively, and computed accelerations at nodes 777, 49 and 383 (Fig. 3) along the crest were compared with accelerograph readings obtained at stations 14–16, 20–22 and 4–5.

SOIL PROPERTIES

Tables 1 and 2 show the initial elastic properties and shear strength parameters assigned to each element group in the two- and three-dimensional analyses. The moduli were related to the initial mean overburden pressure in each group by using a total unit weight of 20 kN/m^3 and assuming a value for the lateral earth pressure coefficient. The data shown in Fig. 4 give typical values from a previous analysis (Prevost, Abdel-Ghaffar & Lacy, 1985) in which similar core materials were used. Although the core soil was much less permeable than the shell, its permeability was not as low as might be obtained in a dam with a narrow clay core of virtually incompressible material, and so a compromise Poisson's ratio of 0·45 was assigned. The rock-fill shell material, though saturated on the upstream face, was considered free-draining, so a Poisson's ratio of 0·3 was assumed. The influence of the bulk modulus on the response was not considered to be of prime importance, especially for the funda-

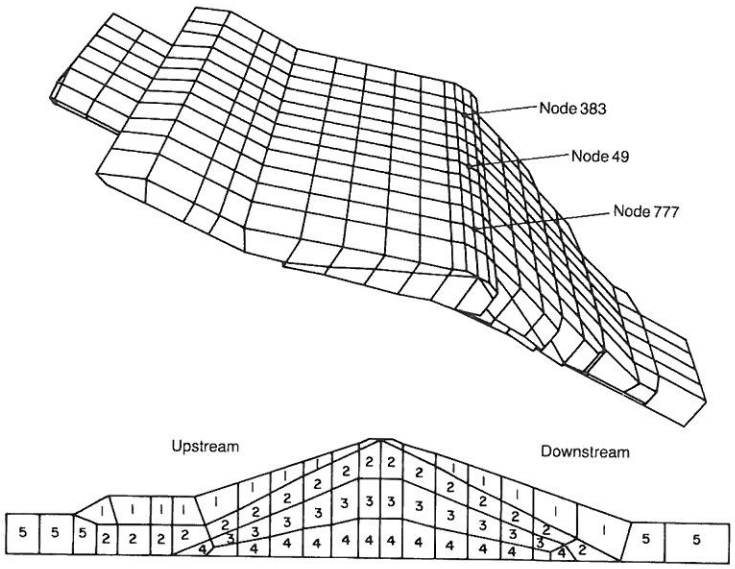

Fig. 3. Mesh used for three-dimensional analyses

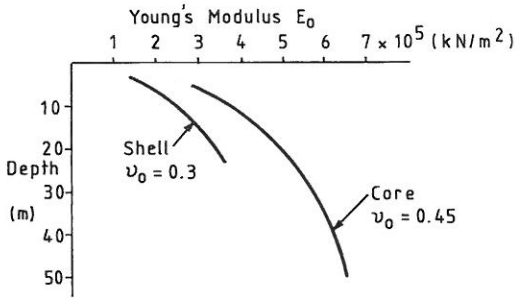

Fig. 4. Stiffness properties of dam materials

mental motion in the up/downstream direction. Its influence on the vertical motion, however, may be more significant and could be investigated through parametric studies.

The core material was assigned $K_0 = 1$, while the shell was given a lower value more appropriate for granular materials where $K_0 = 1 - \sin \phi'$. From the initial mean stress and shear stress within each group (p_0 and q_0) and the shear strength parameters c' and ϕ' a stress path could be assumed and the shear strength estimated. For the core material, an undrained stress path in which $dp/dq = 0$ (i.e. no volume change tendency) was assumed, whereas for the more permeable shell, a drained triaxial stress path in which $dp/dq = 1/3$ was assumed as shown in Fig. 5. In the case of the shell, a drained plane strain stress path would probably be more appropriate. However,

Table 1. Material properties for two-dimensional Long Valley Dam analyses

Group	E_0: kPa	ν_0	ϕ'	c': kPa
1: drained	1·6E5	0·30	40	0
2: drained	2·1E5	0·30	40	0
3: undrained	4·0E5	0·45	39	45
4: undrained	5·0E5	0·45	39	45
5: undrained	5·5E5	0·45	39	45
6: undrained	5·9E5	0·45	39	45
7: undrained	6·2E5	0·45	39	45
8: undrained	6·5E5	0·45	39	45
9: elastic	4·9E6	0·30	—	—

Table 2. Material properties for three-dimensional Long Valley Dam analyses

Group	E_0: kPa	ν_0	ϕ'	c': kPa
1: drained	1·9E5	0·30	40	0
2: undrained	4·3E5	0·45	39	45
3: undrained	5·5E5	0·45	39	45
4: undrained	6·3E5	0·45	39	45
5: elastic	4·9E6	0·30	—	—

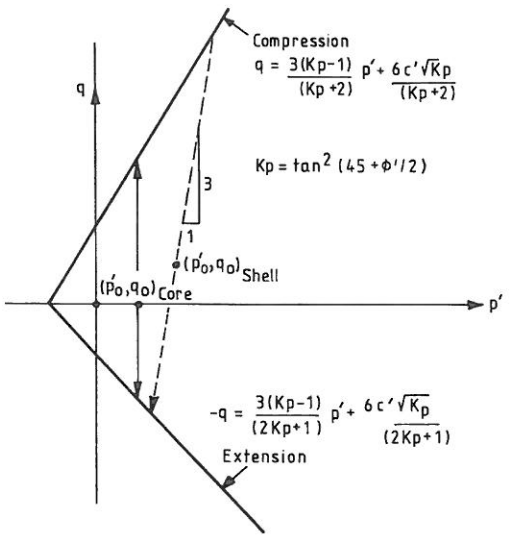

Fig. 5. Calculation for obtaining peak shear strength q_{max}

the shear strength parameters (Tables 1 and 2) were triaxial properties, thus the triaxial stress path assumption is thought to be justified in view of its simplicity and conservative estimates of shear strength.

Knowing the initial gradient and the ultimate strength, a stress–strain curve was then fitted to the data in both compression and extension. The usual method is to use a hyperbola of the form

$$q = \frac{G_0 \bar{\varepsilon}}{1 + \frac{G_0}{q_{max}} \bar{\varepsilon}} \tag{1}$$

An alternative logarithmic function has also been used in the three-dimensional analyses of the form

$$\bar{\varepsilon} = Aq - B \ln\left(1 - \frac{q}{q_{max}}\right) \tag{2}$$

which can be arranged to have the correct initial gradient G_0 where

$$G_0 = \frac{q_{max}}{Aq_{max} + B} \tag{3}$$

By varying A and B, the shape of the curve can be adjusted. Stress–strain curve generation functions such as those given by eqns (1) and (2) are no substitute for actual test data.

Having obtained the stress–strain curve in both compression and extension, a series of cylindrical yield surfaces (Prevost, 1977) could then be generated for use in the multi-surface plasticity model.

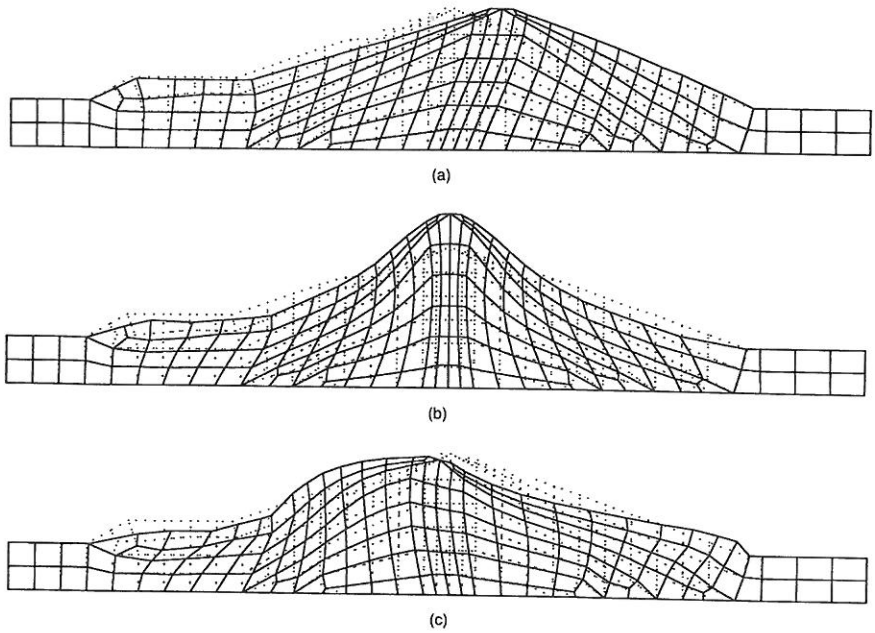

Fig. 6. First three two-dimensional eigenmodes

The present model includes no viscous damping, the main source of damping being hysteretic.

NUMERICAL ALGORITHMS

The eigenvalue analyses used the elastic properties indicated by Tables 1 and 2 together with a lumped-mass discretization in which a density of 2000 kg/m^3 was assumed throughout. The non-linear time-domain analyses used a modified Newton-Raphson approach in which the stiffness matrix was reformed at the beginning of each time-step. Iterations within each time-step were performed until convergence of the stresses onto the appropriate yield surfaces was achieved. Convergence was said to have occurred when the (non-dimensionalized) accelerations from one iteration to the next changed by less than 10^{-3}, and when the out-of-balance force was less than 10^{-3} times its original value at iteration 0. A Newmark time-stepping algorithm was used for the time integrations (Newmark, 1959), with time-stepping algorithm parameters of $\alpha = 0{\cdot}55$, $\beta = (\alpha + \frac{1}{2})^2/4 = 0{\cdot}28$. The slight numerical damping introduced by these values was considered justified, as it is effective in removing spurious high frequencies (present due to the finite element discretization).

EIGENVALUE ANALYSES

The results from the 2- and 3-d analyses are shown in Table 3. Only the first three natural frequencies are presented in each case, and these are compared with values estimated from spectral analysis of the response to earthquake excitation. The computed and measured values give acceptable agreement in both cases, although the 3-d values give closer agreement than the 2-d values. Figure 6 gives the first three 2-d mode shapes, and Fig. 7 the first two 3-d mode shapes. (The third mode shape in 3-d was not included because the 3-d plotter did not give a clear representation.) The fundamental mode shape is clearly an

Table 3. Eigenvalue analyses

Mode number	Resonant frequencies from spectral analysis: Hz	From 2-d FE model	From 3-d FE model
1	1·85	1·76	1·95
2	2·15	2·58	2·20
3	2·45	3·00	2·25

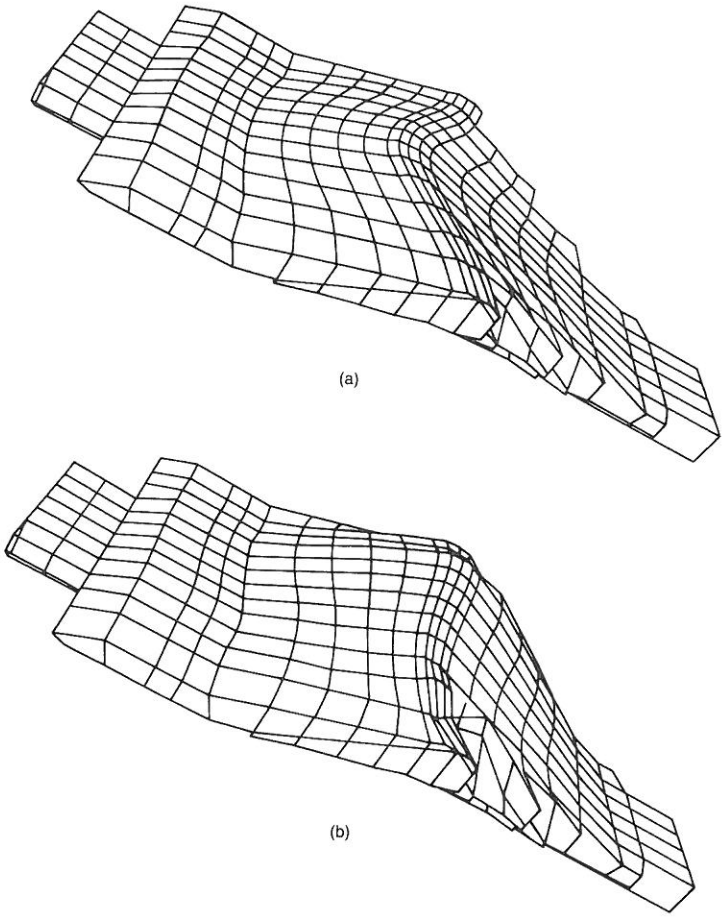

Fig. 7. First two three-dimensional eigenmodes

up/downstream motion with a natural frequency in the range 1·75 Hz–1·95 Hz, but it should be noted that the second and subsequent mode shapes are not necessarily the same in 2- and 3-d. For example, from Fig. 6(b) the second 2-d mode shape implies an almost symmetrical vertical motion whereas the second 3-d mode shape from Fig. 7(b) implies an asymmetric vertical motion along the crest.

TIME DOMAIN ANALYSES

Two dimensions

The accelerographs took their readings at 0·02 s intervals (the same time-step was used in the numerical time-stepping algorithm). Accelerations were applied uniformly to the base of the mesh over a period of 12 s (600 steps).

Figure 8 shows the x acceleration as measured at stations 11 and 20 and indicates the amplification that has occurred between the base and the crest. The peak amplitude at the crest has a magnification factor of about 3 over the peak base amplitude. The computed response of the crest in the up/downstream direction is compared with measured values in Fig. 9. Excellent overall agreement is achieved, with the computed values (solid lines) giving somewhat higher amplitudes. The frequency content of the two time records is compared in the form of a Fourier amplitude spectrum (FAS) in Fig. 9(b). The peaks are in close agreement although the computed values show rather more energy associated with the fundamental frequency around 1·8 Hz.

The response of a single degree of freedom oscillator with 10% damping to the computed and measured acceleration in the up/downstream direction is shown in Fig. 9(c) in the form of a velocity response spectrum (VRS). This plot gives the maximum velocity recorded as a function of the natural period of the oscillator. The curves are in close agreement and give similar informa-

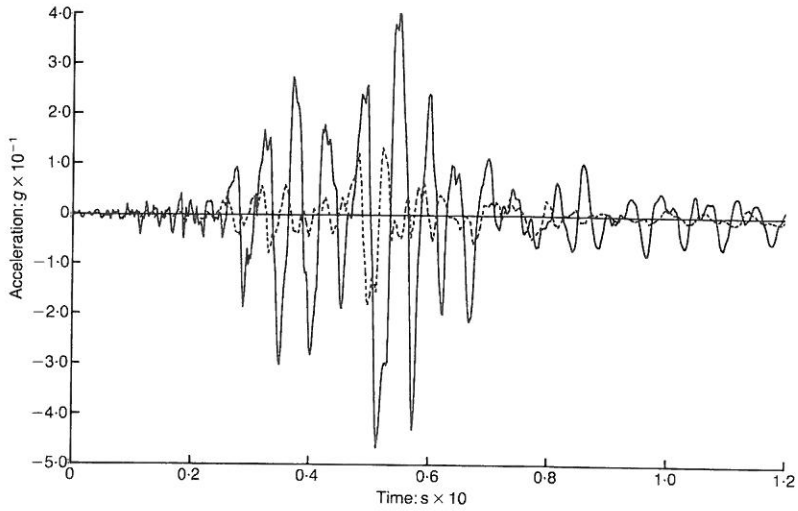

Fig. 8. Measured up/downstream acceleration at base (dashed line) and crest (solid line)

tion to that provided by the Fourier spectrum but in 'smoother' form. An additional comparison of the two records was made by calculating the correlation coefficient r_{xy} where

$$r_{xy} = \frac{s_{xy}}{s_{xx}\, s_{yy}} \tag{4}$$

$$s_{xx}^2 = \frac{1}{n}\sum_{i=1}^{n}(x_i - \bar{x})^2$$

x-sample variance (5)

$$s_{yy}^2 = \frac{1}{n}\sum_{i=1}^{n}(y_i - \bar{y})^2$$

y-sample variance (6)

$$s_{xy} = \frac{1}{n}\sum_{i=1}^{n}(x_i - \bar{x})(y_i - \bar{y})$$

xy-sample covariance (7)

with $\bar{x}$, $\bar{y}$ as the mean values.

Figure 10 shows the 'cumulative' correlation coefficient over field lengths increasing from 0–1 s to 0–12 s. The correlation coefficient is always positive but quite variable over the first six seconds. Over 12 seconds the correlation coefficient settled on a value just greater than 0·42.

An interesting result is shown in Fig. 11 where the effect of shifting one 12 s record relative to the other is observed. Shifts in the range 0–1 s in each direction have been considered, and it is clear that an improvement in the correlation coefficient up to 0·72 can be achieved by a small shift of the origin of the computed values of 0·08 s (i.e. $4\Delta t$).

The calculated acceleration in the vertical direction showed considerably less agreement with measured values. Part of the difficulty is illustrated in Fig. 12 which shows superimposed plots of vertical acceleration at the base and crest measured by stations 13 and 21. This excitation is considerably 'noisier' than in the up/downstream direction and is less intense. The maximum recorded vertical acceleration at the crest is 0·185 g compared with 0·403 g in the up/downstream direction.

The computed accelerations in the vertical direction are compared with measured values in Fig. 13(a). The computed values (solid) show generally greater amplitudes than the measured values (dashed). The Fourier amplitude spectra of these time histories is given in Fig. 13(b) and the measured values indicate a broad band of frequencies with no particular frequency dominating the situation. The computed values also contain a broad band of frequencies, but with clear peaks in the ranges 2–3 Hz and 5–6 Hz. The second eigenmode given in Fig. 6(b) involves vertical motions and has a natural frequency of 2·15 Hz. The peaks of energy occurring in the 5–6 Hz range must correspond to higher eigenmodes. It should be noted, however, that the energy content in the vertical direction is considerably less than in the up/downstream direction, the peaks of the measured Fourier amplitude spectra being of the order 0·08 gs and 0·43 gs respectively.

The velocity response spectrum for vertical motion (Fig. 13(c)) gives velocities that are about an order of magnitude less than those in the up/downstream direction. However, the shape of the two curves agrees quite well with the measured

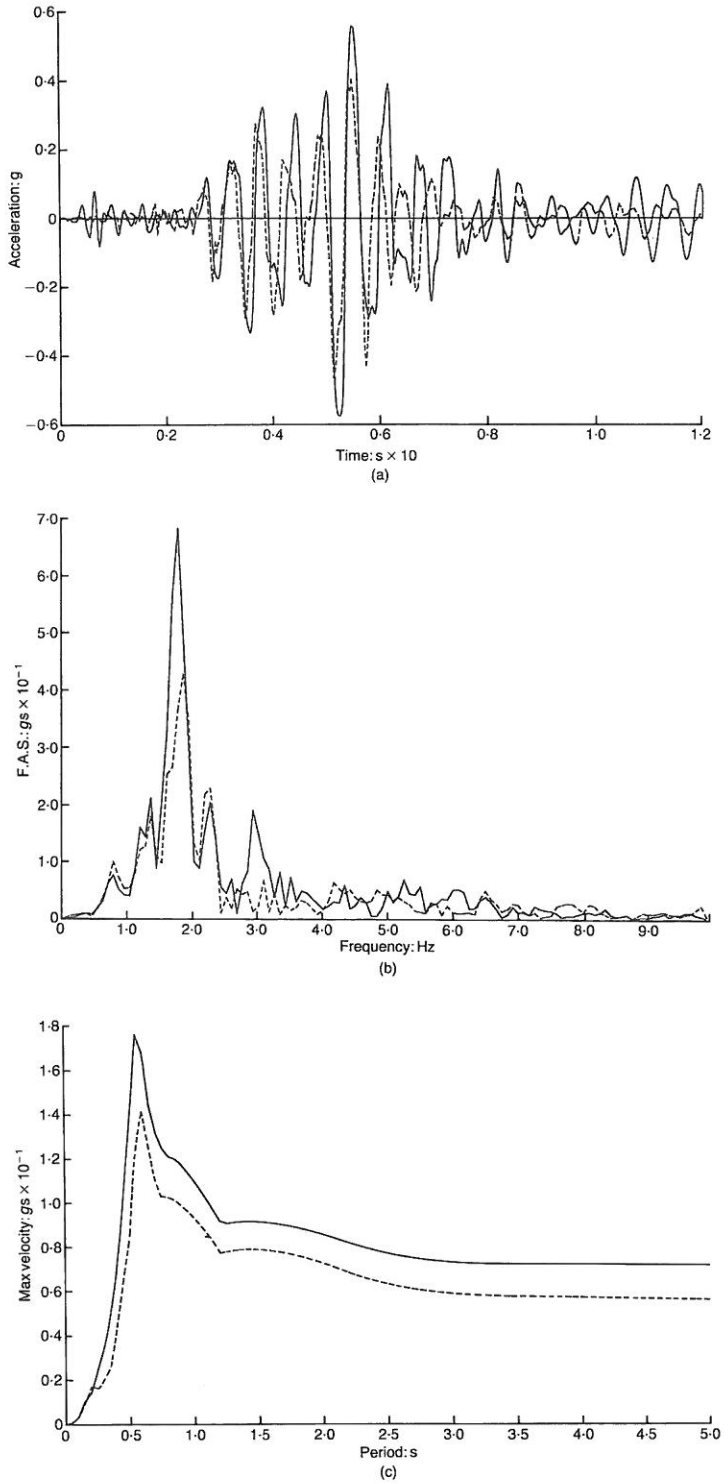

Fig. 9. Computed against measured motion at station 20 (up/downstream, 2-d): (a) acceleration; (b) Fourier amplitude spectrum; (c) velocity response spectrum

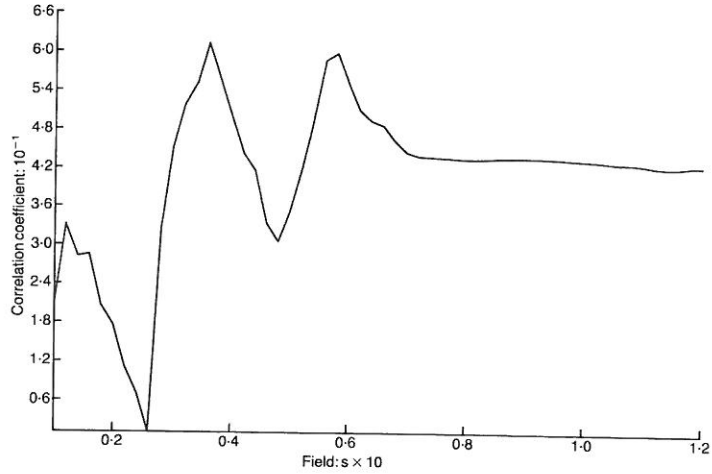

Fig. 10. Cumulative correlation with station 20 (up/downstream, 2-d)

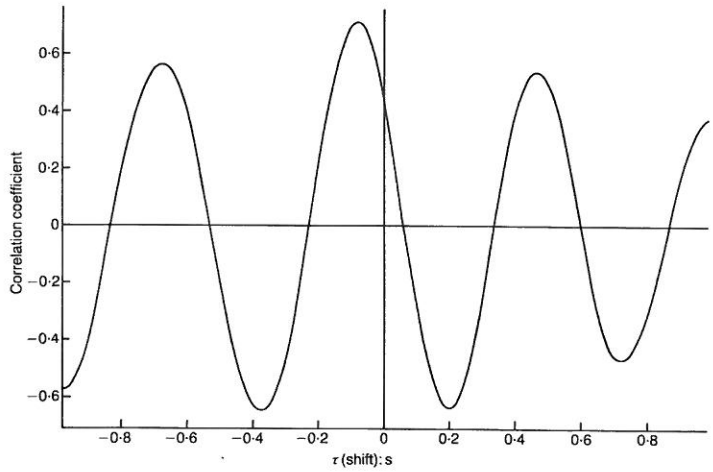

Fig. 11. Effects of shifting on correlation with station 20 (up/downstream, 2-d)

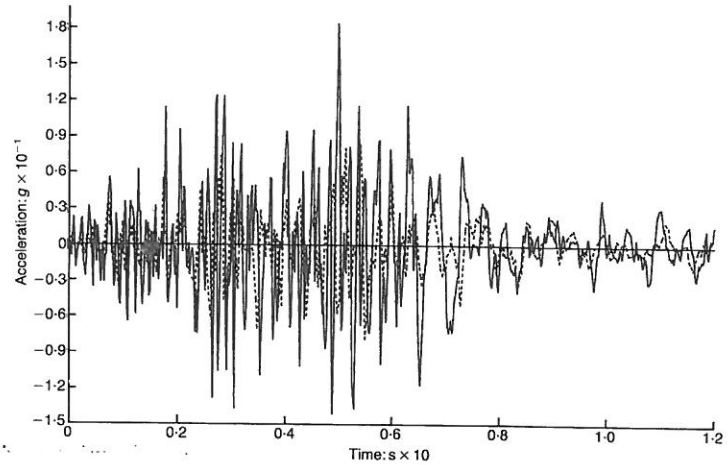

Fig. 12. Measured vertical acceleration at base (dashed) and crest (solid)

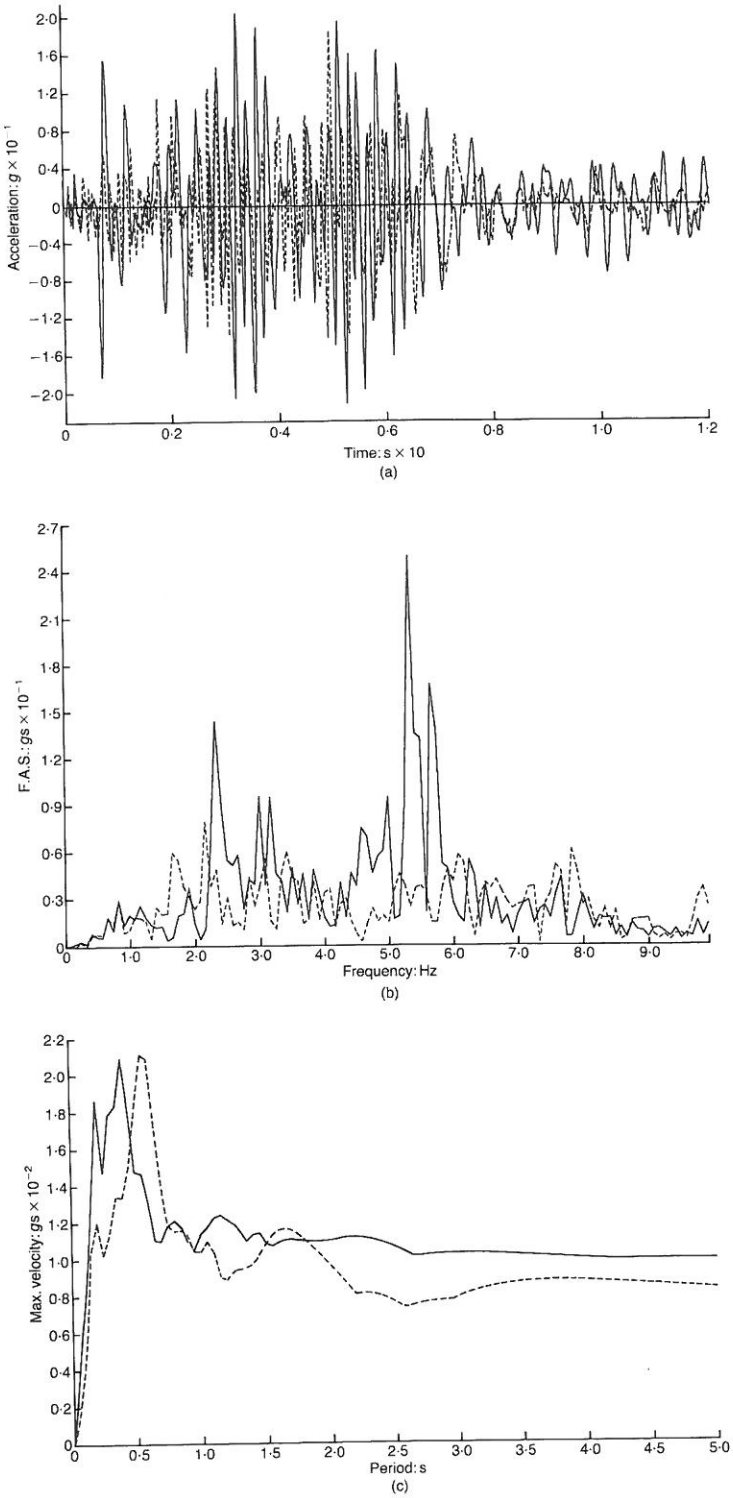

Fig. 13. Computed against measured motion at station 21 (vertical, 2-d): (a) acceleration; (b) FAS; (c) VRS

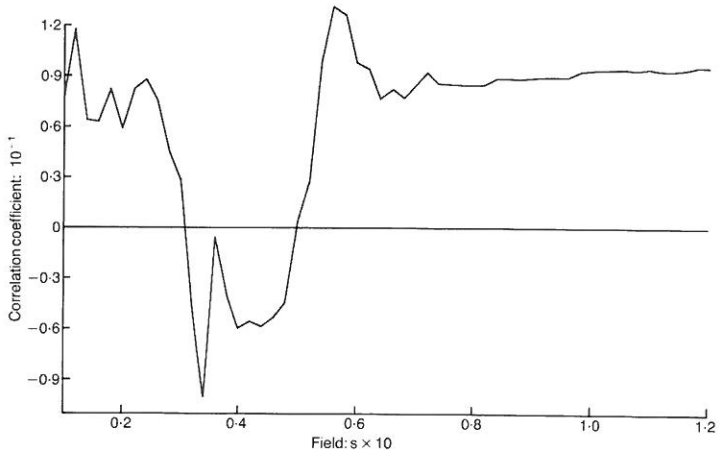

Fig. 14. Cumulative correlation with station 21 (vertical, 2-d)

values, showing a slightly higher natural period than the computed values. The correlation between measured and computed vertical acceleration at the crest is rather poor (Figs 14 and 15). In the cumulative case (Fig. 14) the whole record shows a very weak positive correlation of less than 0·1. Similarly, the effects of shifting (Fig. 15) make little improvement, and merely demonstrate the generally higher frequency content of the data.

Three dimensions

Using the same algorithm as in the 2-d case, the computed accelerations at three locations on the crest (as shown in Fig. 3) were compared with the measured values at stations 14–16, 20–22 and 4–5. Figure 16(a) gives the computed and measured acceleration in the up/downstream direction at the crest centreline. As in the 2-d case, very good agreement is achieved, but due to the softer (logarithmic) stress–strain curve employed to generate the yield surfaces, the computed values give lower amplitudes than the measured values. The peak acceleration of 0·45 g occurring between 5 and 6 seconds is well reproduced, however. It would appear that the computed amplitudes are quite sensitive to the shape of the stress–strain curve between its initial gradient of G_0 and its ultimate shear stress of q_{max}. The 'softer' the assumed stress–strain curve, the more hysteresis at low strain levels, and the greater the energy dissipation. This observation suggests that

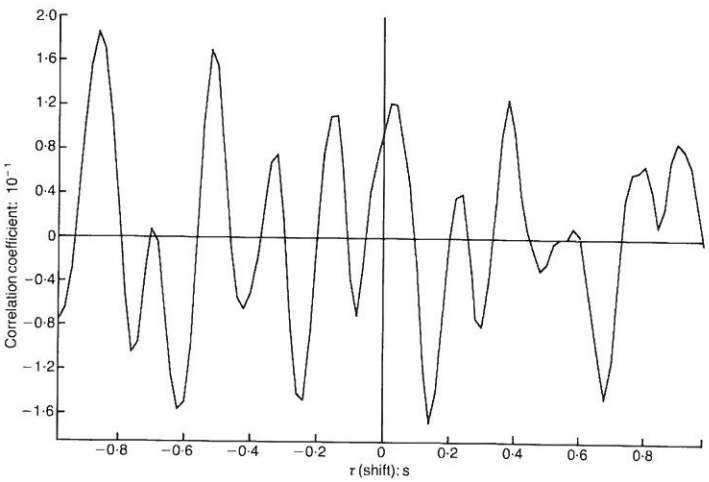

Fig. 15. Effects of shifting on correlation with station 21 (vertical, 2-d)

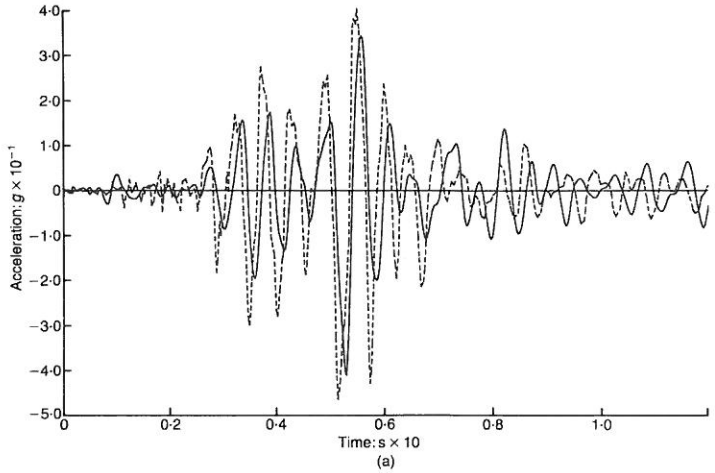

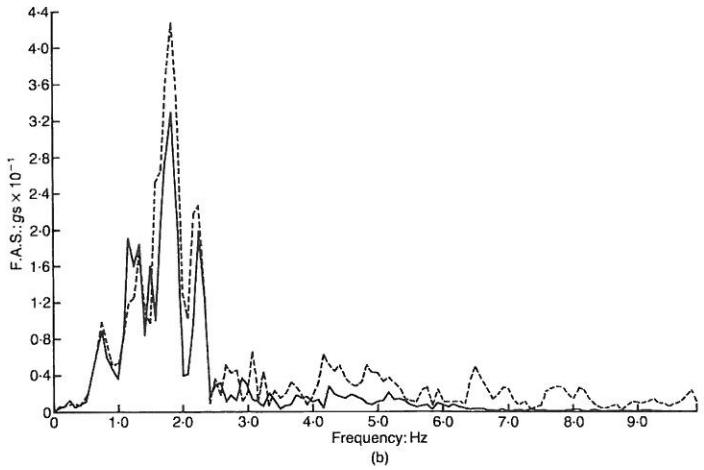

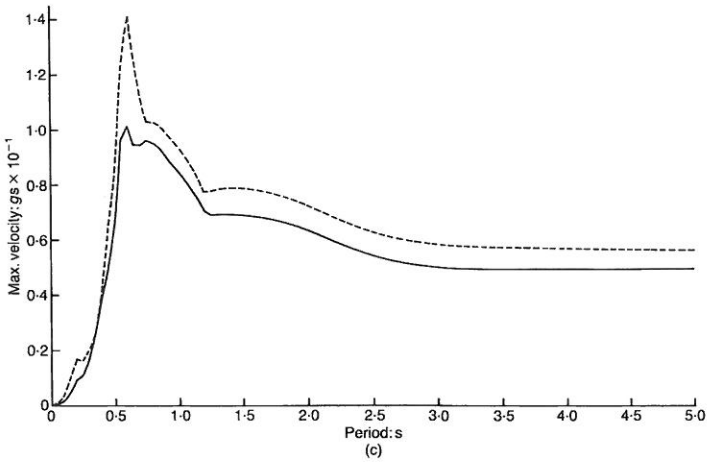

Fig. 16. Computed against measured motion at station 20 (up/downstream, 3-d): (a) acceleration; (b) FAS; (c) VRS

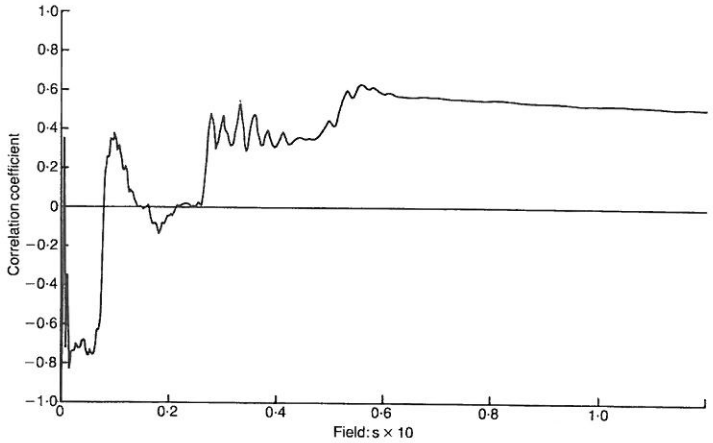

Fig. 17. Cumulative correlation with station 20 (up/downstream, 3-d)

parametric studies involving the shape of the assumed stress–strain curves, and their resulting effect on hysteretic damping, would be of value.

The frequency content of the up/downstream motion is compared in Fig. 16(b) and 16(c) in the form of Fourier and velocity response spectra. These show that the energy is concentrated at a frequency of just under 2 Hz. The correlation coefficient shown in Fig. 17 for the full time history converges on a value around 0·5. The effects of shifting shown in Fig. 18 indicate that a maximum correlation of 0·86 could be achieved. These results represent a small improvement over the 2-d counterparts.

The computed results in the vertical (y) and transverse (z) directions at the crest centreline gave little or no correlation with measured values. The vertical response shown in Fig. 19(a) indicates computed values with substantially lower amplitudes than the measured values. The frequency content of the vertical acceleration in the form of Fourier and velocity response spectra (Fig. 19(b) and 19(c)) indicates that the computed values do not reproduce the higher frequencies present in the broad band of measured frequencies. The same can be said of the computed transverse acceleration shown in Fig. 20.

The computed values of acceleration obtained at other locations on the crest (see Fig. 3) produced a similar pattern. The up/downstream values correlated quite well, but in the other directions the results were disappointing. Figure 21(a) shows the computed values at node 383 compared with the measured values at station 4. The amplitudes are lower than at the centreline as would be expected as the rigid valley wall is approached.

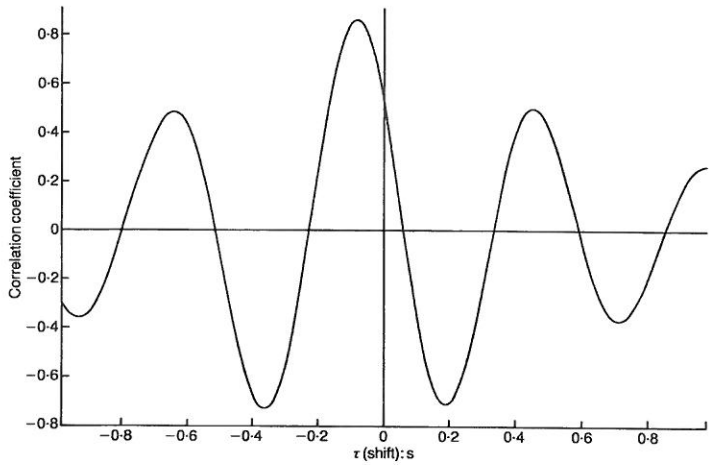

Fig. 18. Effects of shifting on correlation with station 20 (up/downstream, 3-d)

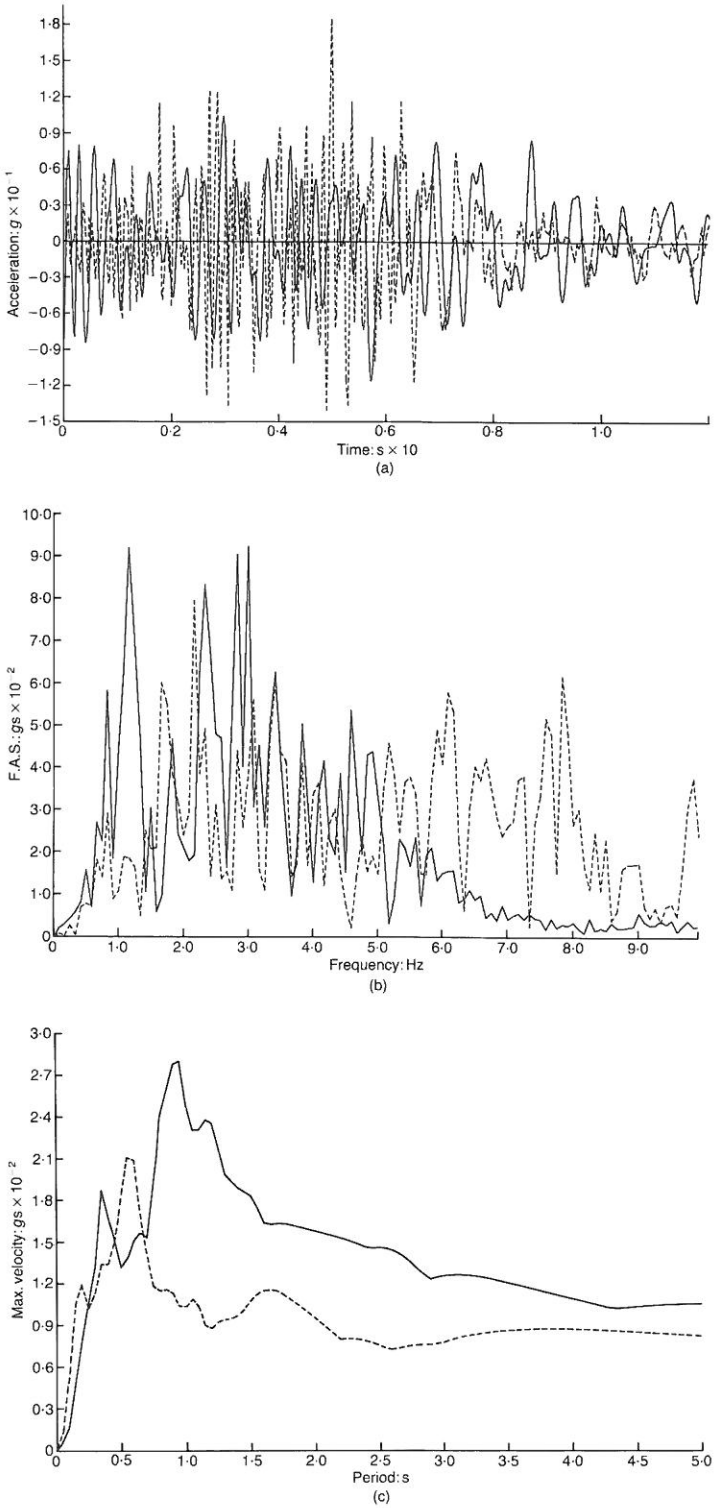

Fig. 19. Computed against measured motion at station 21 (vertical, 3-d): (a) acceleration; (b) FAS; (c) VRS

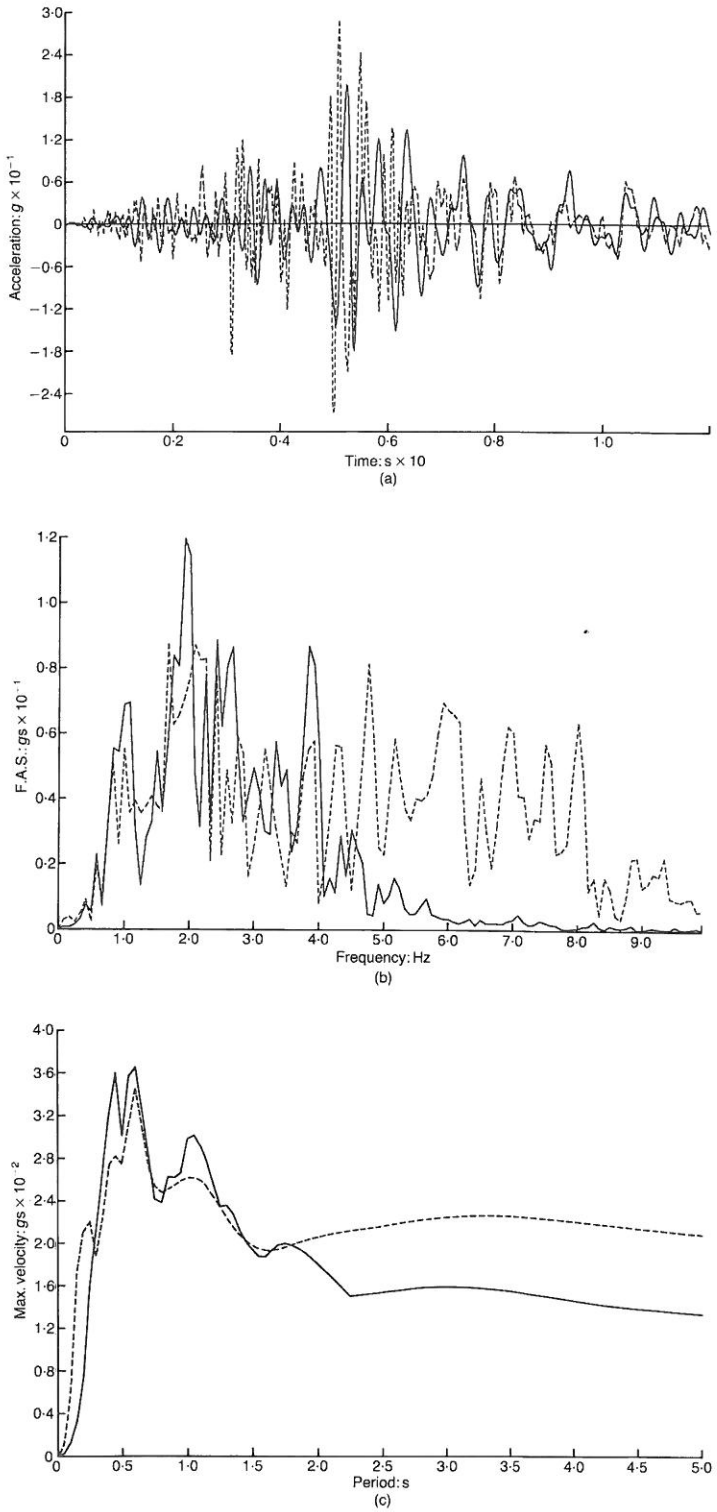

Fig. 20. Computed against measured motion at station 22 (transverse, 3-d): (a) acceleration; (b) FAS; (c) VRS

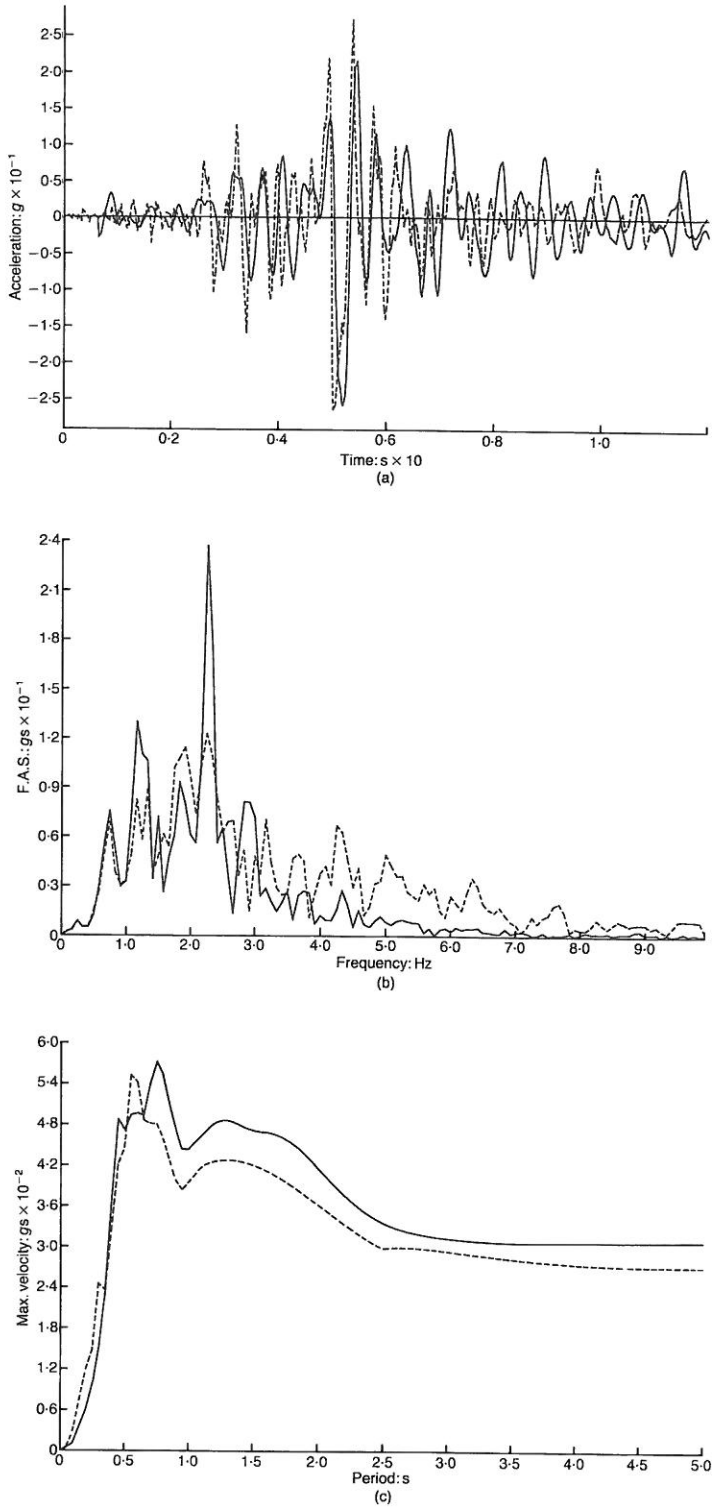

Fig. 21. Computed against measured motion at station 4 (up/downstream, 3-d): (a) acceleration; (b) FAS; (c) VRS

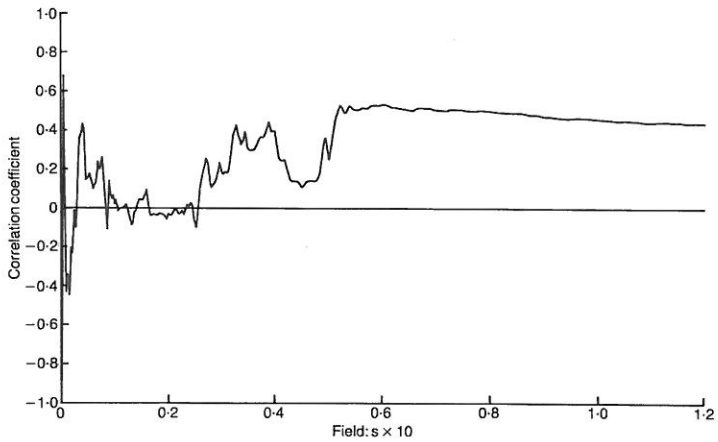

Fig. 22. Cumulative correlation with station 4 (up/downstream, 3-d)

The Fourier and velocity response spectra are given in Fig. 21(b) and (c) and show that the frequency content is quite well reproduced. The correlation coefficient for the full time history converges on a value of around 0·43 (Fig. 22) whereas the effects of shifting (Fig. 23) indicate that a correlation as high as 0·68 could be achieved.

The vertical accelerations computed at node 383 (solid lines) are compared with the measured values at station 5 (dashed lines) in Fig. 24(a) and show poor agreement in the frequency content. The amplitude levels are in general agreement, however. The Fourier spectrum for these results (Fig. 24(b)) confirms that the measured values contain more high frequencies that could be captured by the finite element analysis. No measured values were available in the transverse (z) direction at this location.

Corresponding to the other side of the crest, computed results at node 777 (see Fig. 3) were also compared with measured values at stations 14, 15 and 16. In the up/downstream direction (Fig. 25) the computed values underestimated the peak acceleration measured at station 14 but the frequencies were reasonably well reproduced as shown by the Fourier and velocity response spectra (Figs 25(b) and 25(c)). The correlation coefficient for the full time history was about 0·43, but shifting of the data could improve this value to 0·56 (Figs 26 and 27).

Comparisons of computed values at node 777 with measured values at stations 15 and 16 in both time and frequency domains are shown in

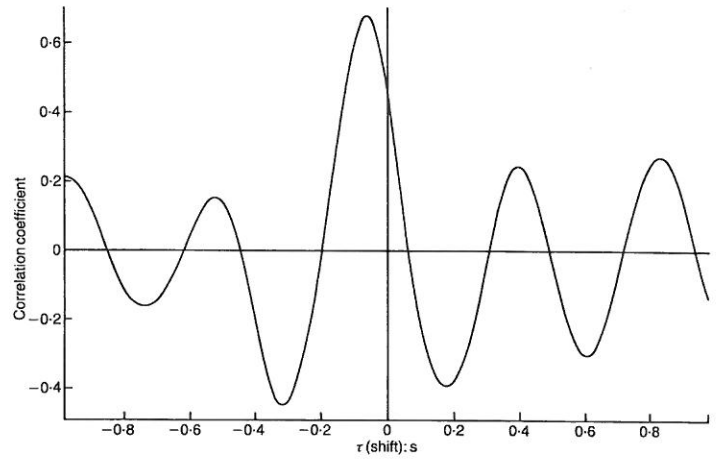

Fig. 23. Effects of shifting on correlation with station 4 (up/downstream, 3-d)

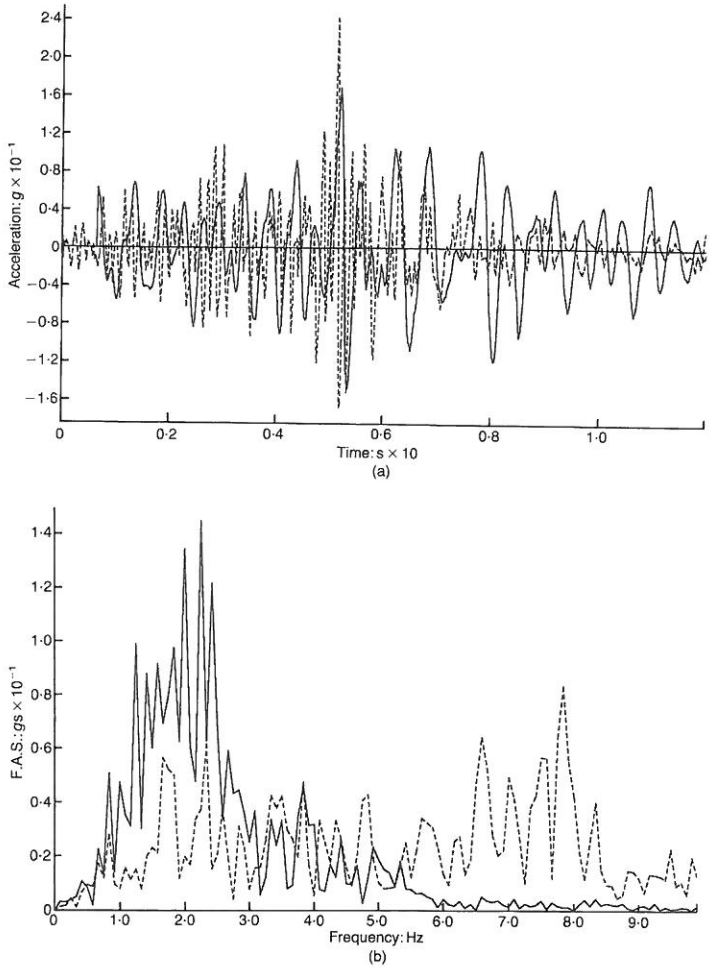

Fig. 24. Computed against measured motion at station 5 (vertical, 3-d): (a) acceleration; (b) FAS

Figs 28 and 29. These follow the same pattern as the previous comparisons, in that the high frequencies of the measured values were not reproduced by the finite element analysis. Although the amplitude levels were of a generally similar order, the acceleration measured at 5 seconds in Figs 28(a) and 29(a) was underestimated by the computed values. It would appear that a stiffer stress–strain curve might increase the computed amplitudes, but possibly at the expense of inadequate hysteretic damping.

It is also possible that the inability of the model to reproduce the higher frequencies was caused partly by the relatively crude finite element discretization used in the 3-d analysis. To deal with this possibility, a finer 3-d mesh has been prepared for further analyses of the Long Valley Dam. The mesh, shown in Fig. 30, uses the 2-d mesh (see Fig. 2) as a parent section and contains a total of 17 sections in the transverse direction. It has 2121 nodes and 1495 elements distributed between 9 element groups.

CONCLUSIONS

Results have been presented comparing the measured and computed behaviour of the Long Valley Dam when subjected to earthquake excitation. Both two-dimensional and three-dimensional analyses were performed and results obtained for the natural frequencies and acceleration time-histories of the crest of the dam. The computed values were compared with natural frequencies estimated by spectral analyses and time-histories measured by a number of accelerographs placed on the dam. Both analyses gave reason-

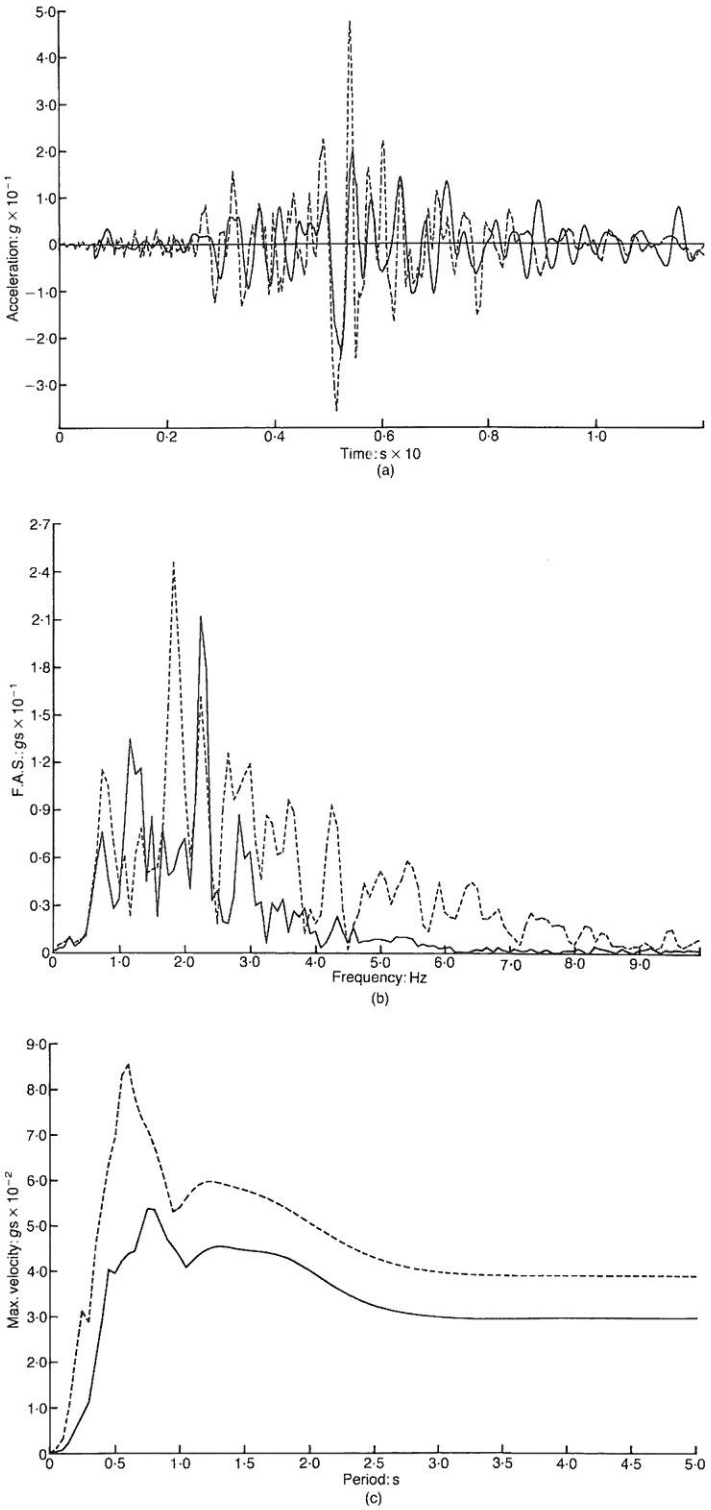

Fig. 25. Computed against measured motion at station 14 (up/downstream, 3-d): (a) acceleration; (b) FAS; (c) VRS

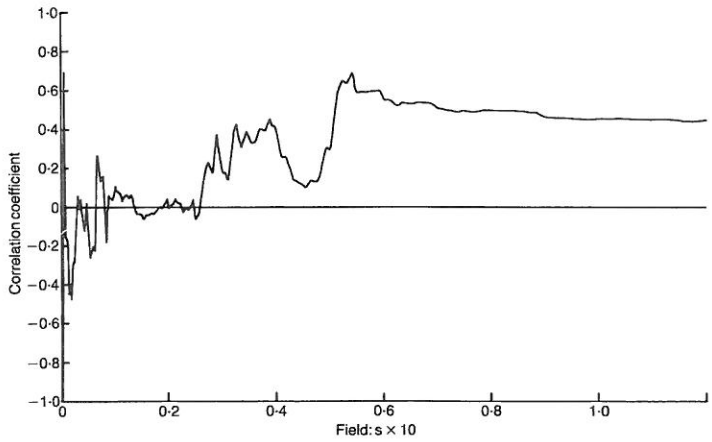

Fig. 26. Cumulative correlation with station 14 (up/downstream, 3-d)

ably close agreement with the natural frequencies of the dam, but the 3-d case performed slightly better. However, care must be exercised when comparing natural frequencies, to ensure that the same mode of vibration is being considered in each case. The finite element frequencies tended to overestimate the measured natural frequencies of the dam due to non-linear effects in the actual structure resulting in degraded stiffness.

A consistent pattern emerged in the acceleration time-histories computed at the crest. In both the 2-d and 3-d analyses, good agreement was obtained between computed and measured values in the up/downstream direction. This was true for both amplitude levels and frequency content. The 3-d results gave marginally better agreement than the 2-d case and showed a potential correlation coefficient of 0·86.

The computed values in the vertical direction in the 2-d analysis, and the vertical and transverse directions in the 3-d analysis, did not give such good agreement. The amplitude levels were of the correct order, but the computed values failed to reproduce the high frequencies present in the measured crest acceleration. This was particularly true in the 3-d analysis. It is suggested that better results might be obtained if a stiffer stress–strain curve was used to model the transition from the initial gradient to peak shear stress q_{max}. However, this might have an adverse effect on the

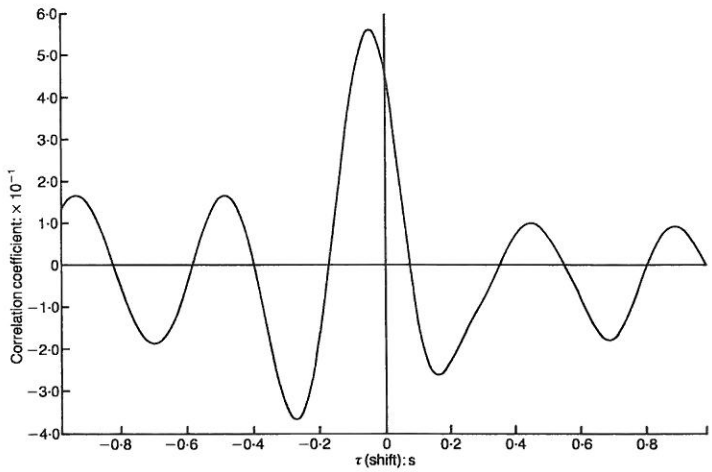

Fig. 27. Effects of shifting on correlation with station 14 (up/downstream, 3-d)

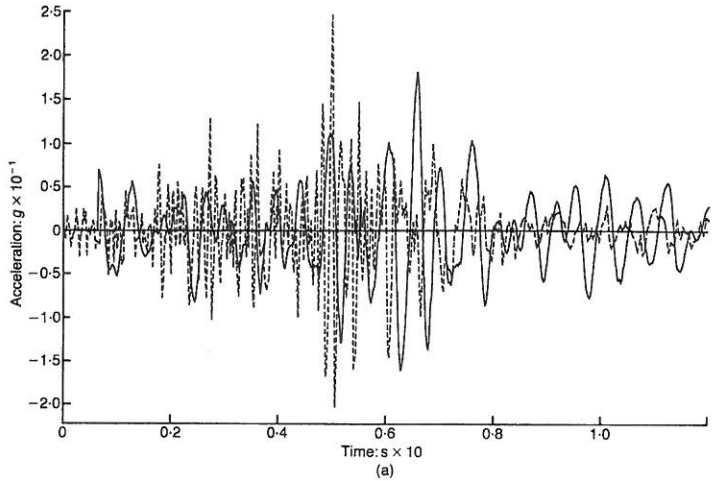

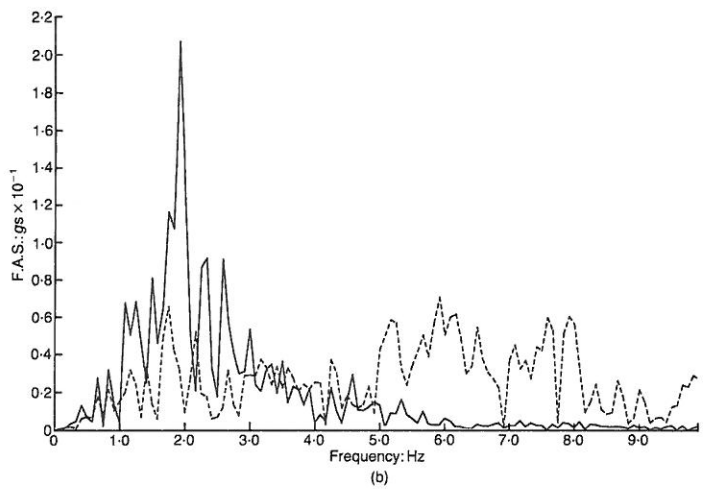

Fig. 28. Computed against measured motion at station 15 (vertical, 3-d): (a) acceleration; (b) FAS

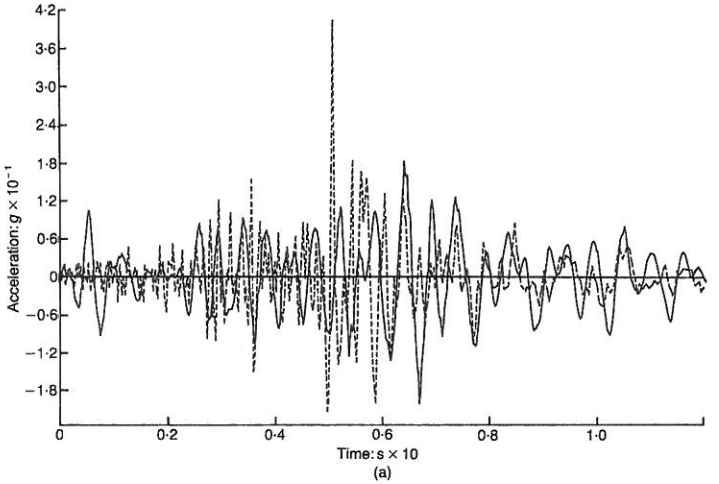

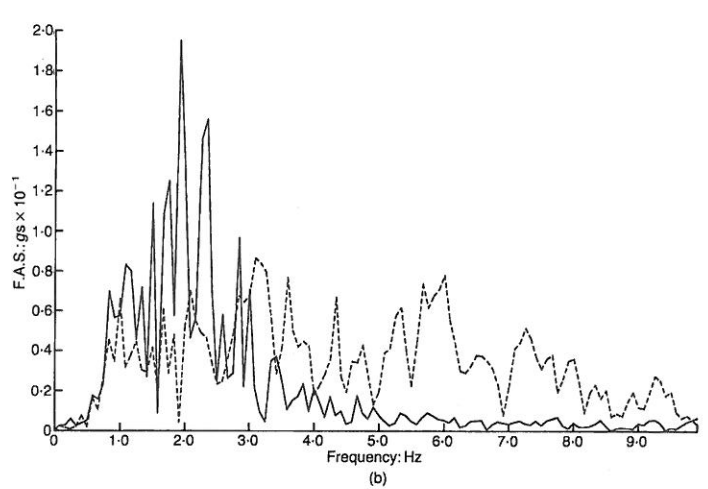

Fig. 29. Computed against measured motion at station 15 (transverse, 3-d): (a) acceleration; (b) FAS

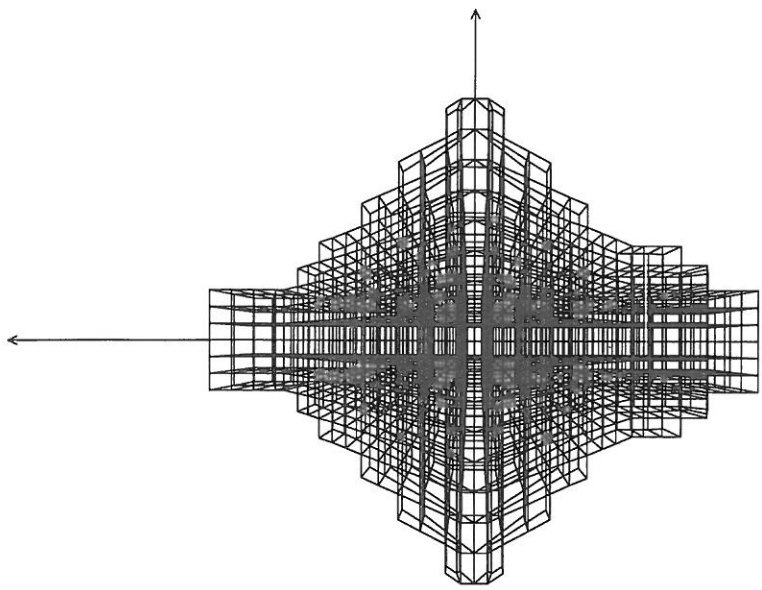

Fig. 30. Skeletal plan view of refined three-dimensional mesh

more important up/downstream results and the reduced hysteretic damping might result in the response failing to attenuate in time.

A further consideration is the ability of the finite element discretization to capture the higher frequencies. In order to further examine this possibility, a considerably finer 3-d mesh has been prepared for further analyses.

ACKNOWLEDGEMENTS

This work was conducted in the Department of Civil Engineering and Operations Research, Princeton University, and was supported by the National Science Foundation under Grant ECE 85-12311, and sub-contract NCEER 86-3034-A5 under the auspices of the National Center for Earthquake Engineering Research. This support is gratefully acknowledged.

REFERENCES

Hoye, W. W., Hegenbart, J. L. & Matsuda, S. (1982). *Long Valley Dam stability evaluations.* Report No. AX 203-24. City of Los Angeles Dept. of Water and Power.

Lacy, S. J. & Prevost, J.-H. (1987). Non-linear seismic response analysis of earth dams. *Soil Dyn. and Earthquake Engng* **6,** No. 1, 48–63.

Lai, S. S. & Seed, H. B. (1985). *Dynamic response of Long Valley Dam in the Mammoth Lake earthquake series of May 25–27 1980.* Report No. UCB/EERC-85/12, Earthquake Engineering Research Center.

Newmark, N. M. (1959). A method of computation for structural dynamics. *J. Mech. Eng. Div. Am. Soc. Civ. Engrs* **85,** EM3, 67–94.

Prevost, J.-H. (1977). Mathematical modelling of monotonic and cyclic undrained clay behaviour. *Int. J. Numerical Analysis Meth. Geomech.* **1,** No. 2, 195–216.

Prevost, J.-H. (1981 and 1987). DYNAFLOW: *a non-linear transient finite element program.* Report 81-SM-1, Civil Engineering Department, Princeton University.

Prevost, J.-H., Abdel-Ghaffar, A. M. & Lacy, S. J. (1985). Non-linear dynamic analysis of an earth dam. *J. Geotech. Eng. Div. Am. Soc. Civ. Engrs* **111,** GT 7, 882–897.

Turpen, C. D. (1980). *Strong motion records from the Mammoth Lake earthquakes of May 1980.* Preliminary Report 27, California Division of Mines & Geology, Sacramento.